Strontium adsorption and desorption reactions in model drinking water distribution systems

Tammie L. Gerke, Brenda J. Little, Todd P. Luxton, Kirk G. Scheckel, J. Barry Maynard and Jeff G. Szabo

ABSTRACT

Divalent cationic strontium (Sr^{2+}) adsorption to and desorption from iron corrosion products were examined in two model drinking water distribution systems (DWDS). One system was maintained with chlorine-disinfected drinking water and the other with the same water with secondary chloramine disinfection. Flow conditions simulated primary transmission lines (constant flow) and residential mains (periods of stagnation). Accumulation of Sr^{2+} to iron corrosion products in model DWDS was independent of disinfection type. Adsorption and desorption mechanisms are discussed. X-ray adsorption near edge structure (XANES) spectroscopy and linear combination fitting determined Sr^{2+} was primarily associated with iron oxyhydroxide corrosion products. At the end of the desorption study, the amount of Sr^{2+} remaining in iron corrosion products equilibrated to approximate levels observed at the end of the constant flow adsorption experiments. These results suggest that enhanced iron corrosion product loading of Sr^{2+} during stagnation could be short lived under constant flow conditions. Differences between adsorption and desorption based on disinfection type (chlorine versus chlorine plus chloramine) cannot be used to control Sr^{2+} desorption.

Key words | calcium carbonate, drinking water distribution system, α-FeOOH, iron, strontium, XANES

Tammie L. Gerke (corresponding author)
Department of Geology and Environmental Earth Science,
Miami University,
USA
E-mail: *gerketl@miamioh.edu*

Tammie L. Gerke
J. Barry Maynard
Department of Geology,
University of Cincinnati,
Cincinnati, OH 45221-0013,
USA

Brenda J. Little
Naval Research Laboratory,
Stennis Space Center, MS 39529,
USA

Todd P. Luxton
Kirk G. Scheckel
U.S. Environmental Protection Agency,
ORD, NRMRL, LRPCD,
Cincinnati, OH, 45268,
USA

Jeff G. Szabo
U.S. Environmental Protection Agency,
NHSRC, WIPD,
Cincinnati, OH 45268,
USA

INTRODUCTION

The World Health Organization (WHO) and the United States Environmental Protection Agency (US EPA) recently recognized the potential for contaminant delivery from drinking water moving through aging drinking water infrastructures. Treated drinking waters use ground or surface waters that transport divalent cationic strontium (Sr^{2+}) as it flows through Sr^{2+}-bearing rocks or soils (Eikenberga *et al.* 2001). Currently, the average Sr^{2+} concentration in United States drinking water is 1.1 mg l^{-1} (Watts & Howe 2010). The US EPA in 2009 set a health reference level for non-radioactive Sr^{2+} daily ingestion by a 70 kg adult at 4.20 mg kg^{-1} (USEPA 2009). In 2010, WHO published a recommended total daily intake limit for non-radioactive Sr^{2+} of 0.13 mg kg^{-1} body weight for an average adult weighing 64 kg (Watts & Howe 2010). As of January 2013 the US EPA requires all public drinking water distribution systems (DWDS) that serve more than 10,000 consumers and 800 additional DWDS that serve 10,000 or fewer consumers to monitor drinking water for specific contaminants including non-radioactive Sr^{2+} (USEPA 2012). If Sr^{2+} water concentration exceeds 0.3 μg l^{-1}, it must be reported to the US EPA. Since the average Sr^{2+} concentration in drinking water in the USA is approximately 1.1 mg l^{-1} it is likely that the drinking water of numerous DWDS will exceed 0.3 μg l^{-1}.

The US EPA guidelines require that water be monitored at the point-of-entry and point-of-maximum residence time (residential mains (RM)) in DWDS because water chemistry

doi: 10.2166/aqua.2014.075

and quality can be altered as water moves through a DWDS (Lin *et al.* 2001; Vikesland & Valentine 2002; Al-Jasser 2007; USEPA 2012). Most DWDS piping is either ductile iron or carbon steel, essentially unalloyed iron. Both materials are susceptible to corrosion and the accumulation of corrosion products on the interior pipe surfaces. Iron corrosion products can serve as reactive sinks for contaminants such as vanadium, lead, copper, arsenic, and zinc (Friedman *et al.* 2010; Gerke *et al.* 2010; Peng & Korshin 2011; Peng *et al.* 2013). Because of this adsorption phenomenon, it is possible to have lower metal concentrations in drinking waters at point-of-maximum residence time compared to point-of-entry drinking waters (Lin *et al.* 2001).

It is well established that pH and disinfectant concentration in drinking water can decrease during periods of stagnation, i.e., minimal to no water flow (Al-Jasser 2007). These parameters can also decrease as water flows through a DWDS (Vikesland & Valentine 2002). Lower pH or disinfection concentration can cause redox reactions of elements in mineral phases within the surface layers of iron corrosion products (Vikesland & Valentine 2002) jeopardizing the structural integrity of these layers (Sedlak & von Gunten 2011). The impact to surface layer integrity can be so extensive that when flow is introduced after stagnation in RM, high concentrations of metal ions, oxyanions and metal-rich particulate matter can be released in close proximity to consumer taps (Gerke *et al.* 2013). Gerke *et al.* (2013) documented this scenario for Sr^{2+}-enriched iron corrosion products in RM and premise plumbing from four fully operational DWDS, each with a distinct water chemistry. Two of the utilities used chlorine and two used secondary chloramine disinfection.

Gerke *et al.* (2013) did not directly evaluate the impact of changes in water chemistry on Sr^{2+} adsorption or desorption from iron corrosion products in a DWDS. Thus the goal of the present study was to evaluate Sr^{2+} adsorption and desorption mechanisms with iron corrosion products with respect to flow parameters found in model primary transmission lines (PTLs) and RM fed with chlorine- or chlorine and secondary chloramine-disinfected drinking water, which had a Sr^{2+} concentration of 0.30 mg l^{-1}. PTLs experience continuous flow whereas RM are subjected to periods of stagnation. Model DWDS were used to simulate both flow conditions. Samples were examined using traditional physiochemical characterization techniques and speciation of Sr^{2+} binding was conducted using synchrotron-based X-ray adsorption near edge structure (XANES) spectroscopy.

MATERIALS AND METHODS

Model DWDS: experimental conditions and sample preparation

Each model DWDS was maintained in a 1 l annular reactor (AR) (BioSurface Technologies, Bozeman, MT). Chlorine-disinfected drinking water was fed to ARCL2. A separate pipe fed the same drinking water with secondary chloramine disinfection added prior to entering into ARNH2Cl. Throughout the reminder of the paper, water with the secondary chloramine treatment will be identified as chloramine-disinfected or chloramine-treated water. For experiments requiring constant water flow through the ARs, the rate was 18 l h^{-1} (approximately 4.75 gallons per minute) (Shaw *et al.* 2012), resulting in a 0.06 h mean retention time. The retention time maintained an average free chlorine residual of 1 mg l^{-1} and a chloramine residual of 2 mg l^{-1} as target goals for a typical DWDS. The drinking water chemistry is presented in Table 1 and was at or near the calcite saturation index.

At the start of the AR experiments, 20 polycarbonate slides were inserted into each AR with each polycarbonate

Table 1 | Selected water quality parameters of finished drinking waters used in the model drinking water distribution systems

Parameter	Chlorine-disinfected water	Chloramine-disinfected water
pH	8.3	8.0–8.3
Hardness (mg l^{-1} as $CaCO_3$)	91–177	91–177
Alkalinity (mg l^{-1} as $CaCO_3$)	68	68
Chlorine – free (mg l^{-1})	0.97	
Chloramine (mg l^{-1})	–	2
Oxidation-reduction potential (mV)	600–700 (650 avg.)	580–620 (600 avg.)
Phosphate (mg-PO_4 l^{-1})	0.083	0.083
Sr^{2+} concentration (mg l^{-1})	0.30	0.30

slide having three 99% pure iron foils (1 cm × 1 cm × 0.5 mm) adhered with acrylic cement. Seven slides were removed to monitor corrosion product formation. One slide, with three iron foils, was collected at the end of each adsorption and desorption experiment from each AR as described below. Data from remaining slides will be reported elsewhere. The adsorption and desorption experiments for ARCL2 and ARNH2Cl included the following (Figure 1):

1. An adsorption experiment simulating PTL was conducted over a 68-day period. The flow rate for the PTL experiment was 18 l h^{-1} and Sr^{2+} concentration was 0.30 mg l^{-1} for both the chlorine- and chloramine-disinfected waters. The inner drum of each AR rotated at 100 rpm producing a shear on the iron foils similar to a flow rate of 0.3 m s^{-1} in a 15.2 cm diameter pipe. At the end of 68 days, one polycarbonate slide was collected (see 'Iron corrosion product sample collection, preparation and analysis' section below for handling details).
2. An adsorption experiment simulating RM commenced immediately after the 68 day PTL experiment and included halting the flow of either chlorine- or chloramine-disinfected water to the ARs while continuing the inner drum rotation at 100 rpm. The RM pipe simulations included a 1-hour stagnation period with exposure to a 100 mg l^{-1} Sr^{2+}-enriched solution (strontium chloride, 99.99%, Fisher Scientific, Pittsburgh, PA). The Sr^{2+}

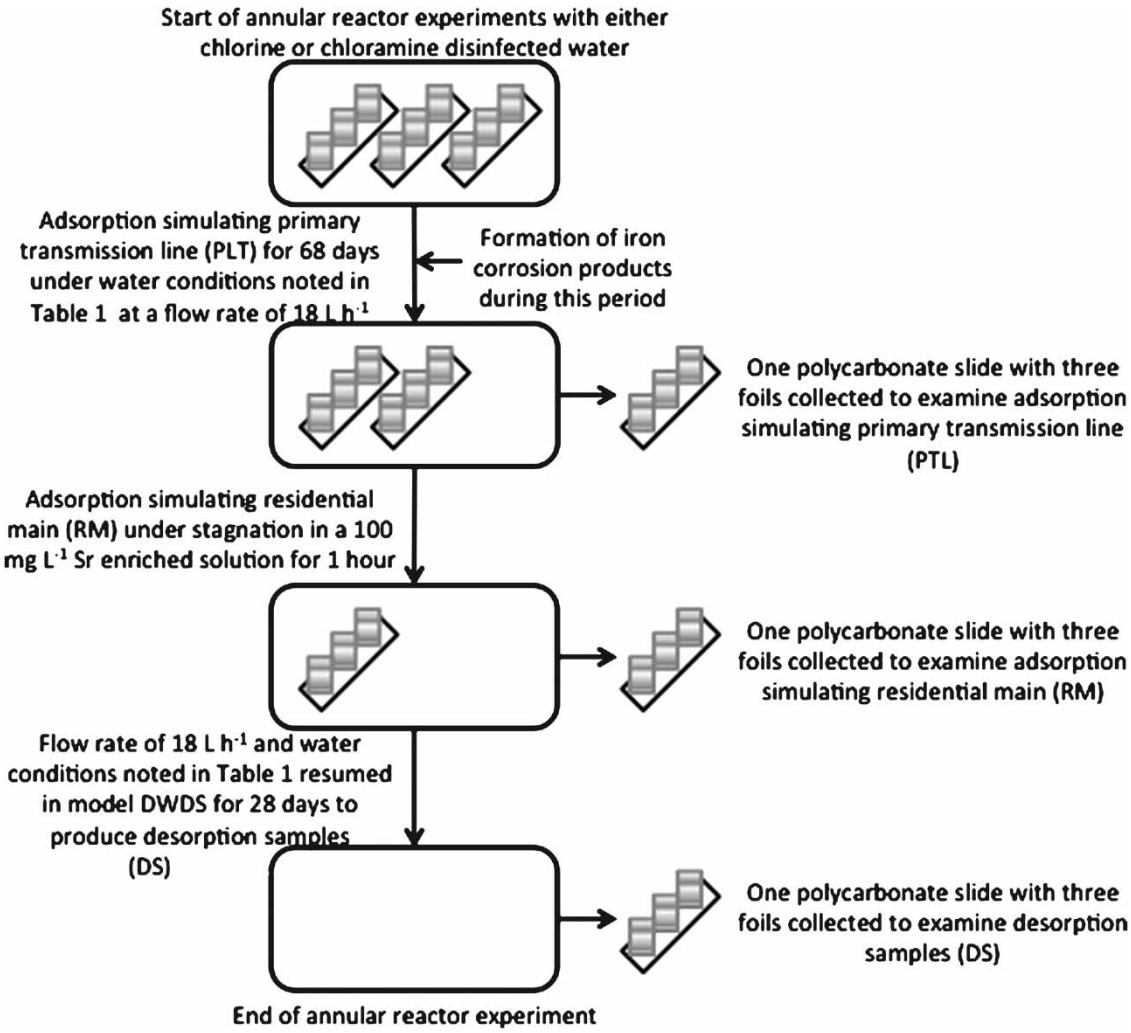

Figure 1 | Schematic of model drinking water distribution systems, slide with iron foils, and sampling events.

concentration for the Sr^{2+}-enriched solution prior to and after injection into the ARs was confirmed using inductively coupled plasma optical emission spectroscopy (ICP-OES, Optima 2100 DV, PerkinElmer, Waltham, MA). Calibration, quality assurance checks, and the water analyses were conducted following the protocol of Szabo *et al.* (2009). Immediately after the 1-hour stagnation, one polycarbonate slide with three iron foils was collected from ARCL2 and ARNH2Cl.

3. The desorption experiment was initiated directly at the end of the 1-hour RM adsorption study. Desorption samples (DS) resulted from resumption of water flow and water conditions used in the PTL adsorption study. After 28 days, a polycarbonate slide with three iron foils was collected from each AR.

Throughout the remainder of this paper, the abbreviations PTL, RM and DS refer to samples collected from adsorption and desorption studies in the model DWDS described above.

Iron corrosion product sample collection, preparation and analysis

After each sampling event, the polycarbonate slide with three foils and associated corrosion products was air dried for at least 72 hours. Digital images were obtained for a representative iron foil from each slide using a Canon G3 digital camera. Iron corrosion product colors were determined using color charts of Cornell & Schwertmann (2003). Solids were removed from all three iron foils of each slide with a metal spatula, combined, ground by hand with an agate mortar and pestle to an approximate grain size of 5 to 10 microns and thoroughly mixed.

An aliquot of each sample was used for mineralogical analysis by powder X-ray diffraction (XRD). Samples were analyzed using a Siemens D-500 automated diffractometer equipped with a Cu Kα tube set at 30 mA and 40 kV (Department of Geology, University of Cincinnati, Cincinnati, OH) following the protocol of Gerke *et al.* (2013).

Approximately 0.15 to 0.25 g of each of the remaining samples was thoroughly mixed with 1.35 to 2.25 g of cellulose and pressed into 31 mm pellets for chemical analysis via X-ray fluorescence. The 31 mm pressed pellets were analyzed for major oxides and trace elements using a Rigaku 3070 X-ray fluorescence spectrometer (Department of Geology, University of Cincinnati, Cincinnati, OH). The protocol of Gerke *et al.* (2010) was used to convert intensity data to percent (by weight) or mg kg^{-1}.

The remaining portions of adsorption and DS were prepared for XANES analysis. Samples were prepared as pellets and sealed between pieces of Kapton tape (Unline, Pleasant Prairie, WI).

X-ray absorption near edge structure run conditions and analysis

XANES studies were performed in top-up mode at 7 GeV with a ring current of 101 mA at beamlines XOR/PNC 20 BM-B (Heald *et al.* 1999) and MRCAT Sector 10 (Segre *et al.* 1999; Kropf *et al.* 2009) of the Advanced Photon Source (APS), Argonne National Laboratory (Argonne, IL). The pre-monochromator slit width was set to 0.5 mm and the Si(III) double crystal monochromator was detuned by 10% to reject higher-order harmonics. The monochromator beam energy position was calibrated by assigning the first inflection of the absorption edge of $SrCl_2$ to 16,105 eV following the protocol of O'Day *et al.* (2000).

Three to six Sr *K*-edge XANES scans were collected for each sample and standard at ambient temperature in fluorescence mode with a solid-state 4-element Si-drift detector. Sr^{2+} adsorbed to α-FeOOH (goethite), γ-FeOOH (lepidocrocite), Fe_3O_4 (magnetite), and $CaCO_3$ (calcite; see Gerke *et al.* 2013), and a Sr^{2+} substituted $CaCO_3$ spectrum (obtained from the Lytle database, http://ixs.iit.edu/database/) were used as standards. All sample and standard spectra were aligned to $SrCl_2$ (99.99%, Fisher Scientific, Pittsburgh, PA) on the same energy grid, averaged, normalized, and the background removed by spline fitting using IFEFFIT (Ravel & Newville 2005). The XANES scans for the DWDS adsorption and DS were smoothed for three iterations using an IFEFFIT smoothing algorithm.

The first derivative of the normalized XANES spectra of the standards and samples was used for all linear combination fitting (LCF). Levenberg–Marquardt least squares algorithm was applied to a fit range of −20 to 80 eV and each LCF analysis encompassed 130 to 221 data points of a given sample spectrum against all five standard spectra.

Best-fit scenarios, defined as having the smallest residual error, also had sums of all fractions close to 1. To fully describe any particular sample within 1% reproducible error, a minimum of two components was necessary, and results have a ±10 percent accuracy.

RESULTS

Physicochemical characteristics of PTL iron corrosion products and associated Sr^{2+} adsorption mechanism

Chlorine-disinfected model DWDS

Iron corrosion products in the chlorine-disinfected model DWDS were flute-shaped, compact dense material (Figures 2(a)–2(c)), composed mainly of γ-FeOOH and lesser amounts of α-FeOOH and Fe_3O_4. Strontium concentration in the corrosion products on the chlorine-treated PTL sample was 22 mg kg^{-1} (Table 2). Elemental composition of the corrosion product is provided in Table 2. The Sr *K*-edge XANES spectrum for the chlorine-disinfected PTL sample had two prominent peaks at 16,110 and 16,147.8 eV (Figure 3(a)). Graphical representation of the calculated LCF (red line) compared to the XANES data (blue line) is presented in Figure 4(a). The LCF results indicated that 8% of Sr^{2+} was incorporated into $CaCO_3$ and 10% of Sr^{2+} was adsorbed to $CaCO_3$, 35% of the Sr^{2+} was adsorbed to α-FeOOH and 47% of the Sr^{2+} was adsorbed to γ-FeOOH (Table 3).

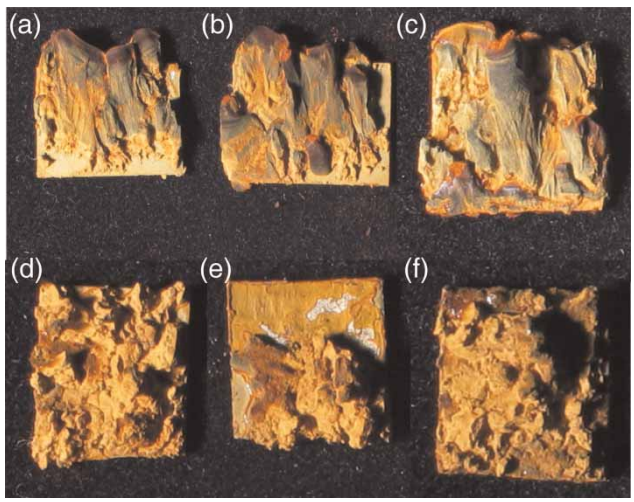

Figure 2 | Images of representative iron corrosion products from (a) chlorine-disinfected PTL, (b) chlorine-disinfected RM, (c) chlorine-disinfected DS, (d) chloramine-disinfected PTL, (e) chloramine-disinfected RM, and (f) chloramine-disinfected DS.

Table 2 | X-ray fluorescence results for the iron corrosion product samples grown in free chlorine and chloramine treated drinking water

Sample ID	Fe %	Ca %	Sr mg kg^{-1}	Pb mg kg^{-1}	Zn mg kg^{-1}	Cu mg kg^{-1}
Chlorine disinfection						
PTL	21.7	0.23	22.0	7.00	20.0	34.0
RM	27.2	0.27	215	10.0	14.0	57.0
DS	28.0	0.27	30.0	12.0	11.0	53.0
Chloramine disinfection						
PTL	23.2	0.50	47.0	14.0	38.0	121
RM	22.2	0.60	217	14.0	47.0	119
DS	23.9	0.50	40.0	19.0	36.0	118

PTL – primary transmission line, RM – residential main, and DS – desorption sample.

Chloramine-disinfected model DWDS

Iron corrosion products formed in the chloramine-disinfected model DWDS were porous and fluffy in appearance (Figures 2(d)–2(f)) and composed primarily of γ-FeOOH with lesser amounts of α-FeOOH and Fe_3O_4. The chloramine-disinfected PTL sample had a Sr^{2+} concentration of 47 mg kg^{-1} (Table 2); more than double the chlorine-treated PTL sample. Elemental composition of the corrosion product is provided in Table 2. The XANES spectrum for the chloramine-disinfected PTL sample had prominent peaks at 16,110 and 16,147.8 eV (Figure 3(a)). The calculated LCF (red line) is compared to the XANES data (blue line) in Figure 4(b). Approximately 15% of the Sr^{2+} was incorporated in $CaCO_3$, 28% of the Sr^{2+} was adsorbed to γ-FeOOH, and 57% of the Sr^{2+} was adsorbed to α-FeOOH (Table 3).

Physicochemical characteristics of RM iron corrosion products and associated Sr^{2+} adsorption mechanism

Chlorine-disinfected model DWDS

The 1-hour stagnation did not influence the morphology or mineralogy of the corrosion products in the chlorine-disinfected

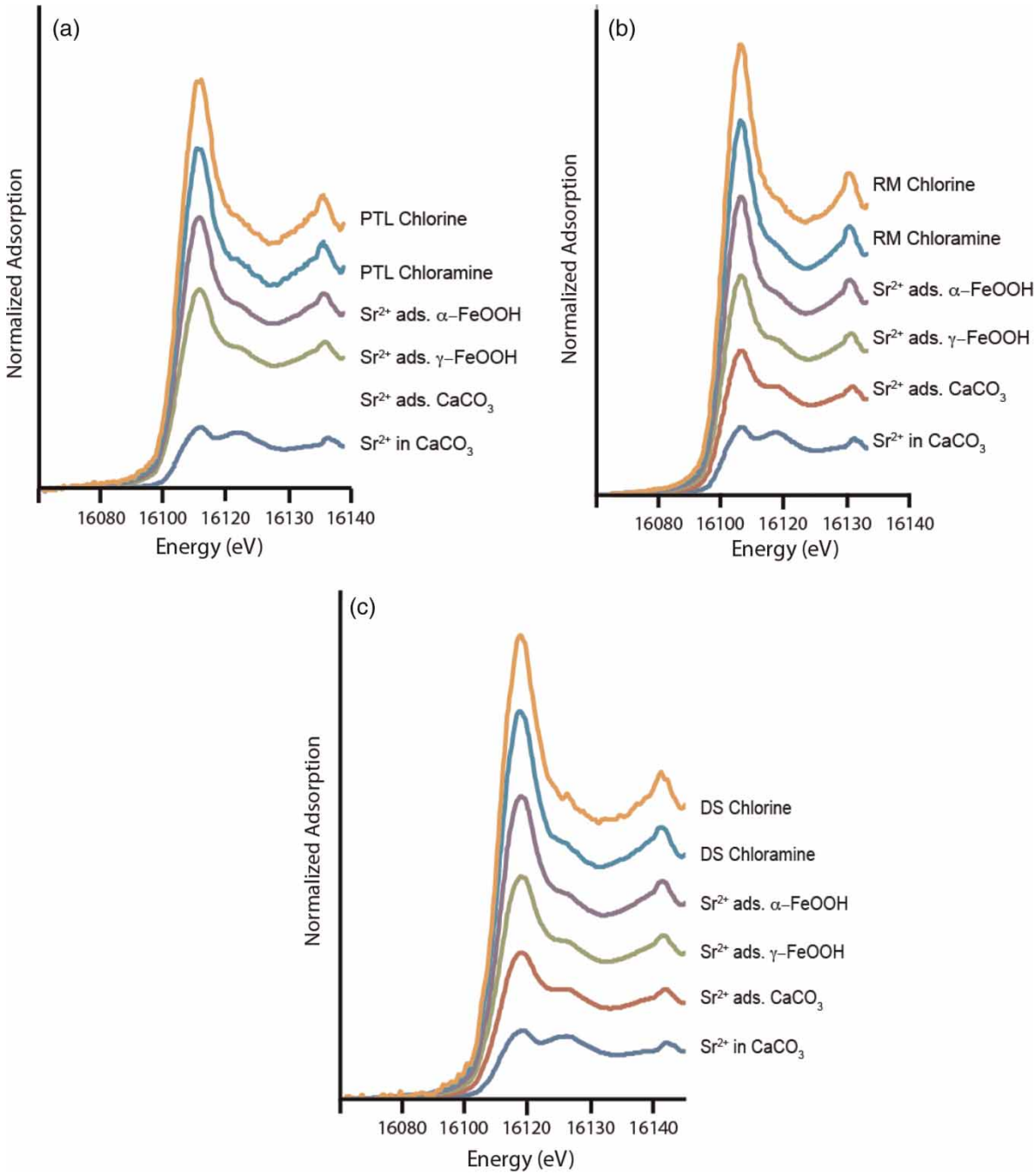

Figure 3 | Strontium *K*-edge spectra for bulk XANES Sr^{2+} standards and for the iron corrosion product samples representing (a) chlorine and chloramine simulated PTL samples, (b) chlorine and chloramine disinfected RM samples, and (c) chlorine and chloramine DS samples. Strontium standards are $CaCO_3$ in which some of the Ca^{2+} sites have been filled with Sr^{2+} (Sr^{2+} incorp. $CaCO_3$) and Sr adsorbed to the following: α-FeOOH (Sr^{2+} ads. α-FeOOH), γ-FeOOH (Sr^{2+} ads. γ-FeOOH), Fe_3O_4 (Sr^{2+} ads. Fe_3O_4), and $CaCO_3$ (Sr^{2+} ads. $CaCO_3$). Please refer to the online version of this paper to see this figure in color: http://www.iwaponline.com/jws/toc.htm.

RM sample (Figure 2(b)). The Sr^{2+} concentration in the chlorine-disinfected RM sample increased from 22 to 215 mg kg^{-1} after a 1-hour exposure to the Sr^{2+}-spiked drinking water (Table 2). The XANES spectrum for the sample had prominent peaks at 16,110 and 16,147.8 eV (Figure 3(b)). Graphical representation of the calculated LCF (red line) compared to the XANES data (blue line) is presented in Figure 4(c). Approximately 2% of the Sr^{2+} was incorporated

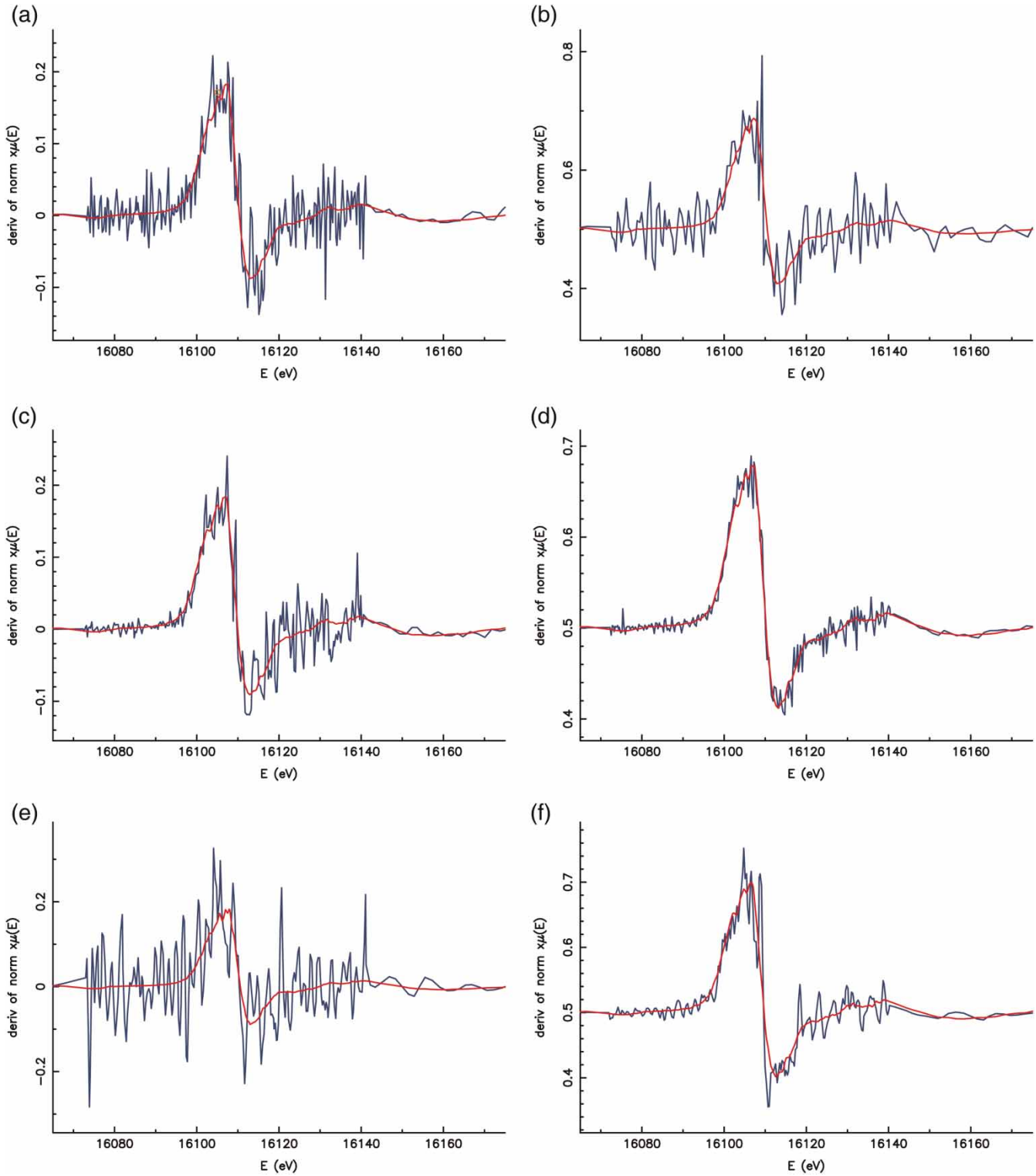

Figure 4 | LCF (red lines) and the first derivative of the normalized mu(E) (blue lines) of the bulk XANES of Sr2þ K-edge spectra for (a) chlorine-disinfected PTL, (b) chloramine-disinfected PTL, (c) chlorine-disinfected RM, (d) chloramine disinfected RM, (e) chlorine-disinfected DS, and (f) chloramine-disinfected DS. Please refer to the online version of this paper to see this figure in color: http://www.iwaponline.com/jws/toc.htm.

Table 3 | LCF results for Sr^{2+} *K*-edge μ-XANES spectra in Figure 4(a). Data presented as weighted percents (±10%) over the fit range of −20 to 80 eV

Sample ID	Sr^{2+} abs. α-FeOOH%	Sr^{2+} abs. γ-FeOOH%	Sr^{2+} abs. $CaCO_3$%	Sr^{2+} incorp. $CaCO_3$	R-factor
Chlorine disinfection					
PTL	35	47	10	8	0.2057
RM	26	72	–	2	0.1547
DS	23	67	–	10	0.5847
Chloramine disinfection					
PTL	57	27.8	–	15	0.2869
RM	57	35	–	9	0.1547
DS	16	77	–	7	0.1390

PTL – primary transmission line, RM – residential main, and DS – desorption sample.

into $CaCO_3$ and 26 and 72% was adsorbed to α-FeOOH and γ-FeOOH, respectively (Table 3).

Chloramine-disinfected model DWDS

Morphology and mineralogy of corrosion products in the chloramine-disinfected RM sample were the same as the chloramine-disinfected PTL sample (Figures 2(d) and 2(e)). The Sr^{2+} concentration in the iron corrosion product increased after a 1-hour exposure to the Sr^{2+}-spiked tap water from 47 to 217 mg kg^{-1} (Table 2). The chloramine-disinfected RM sample had pronounced peaks at 16,110 and 16,147.8 eV in the XANES spectrum (Figure 3(b)). The calculated LCF (red line) is compared to the XANES data (blue line) in Figure 4(d). Approximately 9% of the Sr^{2+} was incorporated into $CaCO_3$ and 35 and 57% of the Sr^{2+} was adsorbed to γ-FeOOH and to α-FeOOH, respectively (Table 3).

Desorption of Sr^{2+} from iron corrosion products

Chlorine-disinfected model DWDS

Morphologically and mineralogically, the chlorine-treated DS sample was identical to the chlorine-treated PTL and RM samples (Figures 2(a)–2(c)). The Sr^{2+} concentration in the iron corrosion products, collected 28 days after drinking water flow resumed, decreased from 215 to 30 mg kg^{-1} (Table 2). The Sr *K*-edge XANES spectrum for the sample had pronounced peaks at 16,110.0 and 16,147.8 eV (Figure 3(c)). Approximately 10% of the Sr^{2+} was incorporated into $CaCO_3$ and 23 and 67% of the Sr^{2+} was adsorbed to α-FeOOH and γ-FeOOH, respectively (Figure 4(e), Table 3).

Chloramine-disinfected model DWDS

Morphologically and mineralogically, the chloramine-disinfected DS sample was identical to the chloramine-treated PTL and RM samples (Figures 2(d)–2(f)). The iron corrosion product collected 28 days after flow resumed had a Sr^{2+} concentration of 40 mg kg^{-1} (Table 2), a decrease from 217 mg kg^{-1}. The XANES spectrum for the sample had prominent peaks at 16,110 and 16,147.8 eV (Figure 3(c)). Approximately 7% of the Sr^{2+} was incorporated into $CaCO_3$ and 16 and 77% of the Sr^{2+} was adsorbed to α-FeOOH and to γ-FeOOH, respectively (Figure 4(f), Table 3).

DISCUSSION

Deterioration of drinking water quality during delivery to a residence has been documented. For example, maintaining a constant disinfectant concentration throughout DWDS is difficult to achieve because drinking water can interact with corrosion products and natural organic matter. Chlorine, the most common disinfectant used in DWDS in United States (Zhang & Edwards 2007), readily reacts with natural organic matter forming carcinogenic disinfection by-products (DBP) such as chloroform (Lin & Valentine 2009; Sedlak & von Gunten 2011). Because DBP concentrations are regulated by the US EPA, drinking water utilities are switching to chloramine disinfection. However, chloramine-disinfected drinking waters have lower oxidation-reduction potentials, compared to chlorine-disinfected waters, making them more corrosive to DWDS infrastructure (Schock & Lemieux 2010). In addition, the switch from chlorine to chloramine can cause massive destabilization of lead corrosion products, i.e., release of lead and other contaminants into drinking water and potential human exposure (Boyd *et al.* 2008; Lin & Valentine 2009; Schock & Lemieux 2010). Red and black water have been attributed to destabilization of iron corrosion products in DWDS. However, there are limited data on the impact of

disinfectant on metal ion adsorption and desorption with iron corrosion products (Friedman *et al.* 2010; Peng & Korshin 2011; Peng *et al.* 2013).

The disinfectants and flow regimes used in the ARs were consistent with those found in fully operational DWDS (Sarin *et al.* 2004; Gerke *et al.* 2008; Teng *et al.* 2008). Furthermore, the corrosion products that formed on the iron foils were typical of DWDS. Well-developed iron corrosion products are primarily iron oxides/oxyhydroxides such as Fe_3O_4, α-FeOOH, and γ-FeOOH and may contain accessory phases such as $CaCO_3$ and SiO_2 (quartz) (Lin *et al.* 2001; Sarin *et al.* 2004; Tang *et al.* 2006; Tamura 2008). Corrosion products in both AR systems were predominantly γ-FeOOH and α-FeOOH and some Fe_3O_4. There were no differences in the proportions of these phases regardless of disinfection or type of sample, i.e. PTL, RM, or DS. $CaCO_3$ was not detected by XRD analysis even though the water used in this study was near or at the calcite saturation index (Table 1). Corrosion products in the chlorine-disinfected system were compact and those that formed in the chloramine-treated system were fluffy. Corrosion product morphology did not change in either system as the experiments progressed from constant flow (PTL) to stagnation (RM) to resumption of flow (DS).

Adsorption mechanisms in the chlorine-disinfected model DWDS

In the chlorine-disinfected PTL samples, Sr^{2+}preferentially adsorbed to γ-FeOOH compared to α-FeOOH, 47 to 35%, respectively (Table 3). This was also observed in the samples from the RM conditions where Sr^{2+} adsorption to γ-FeOOH was greater, 72%, compared to 26% Sr^{2+} adsorption to α-FeOOH (Table 3). Once flow resumed, the distribution of Sr^{2+} adsorption species remained similar to the RM samples, i.e., more Sr^{2+} adsorbed γ-FeOOH over α-FeOOH (67 versus 23%, respectively) (Table 3). Changes that occurred in the water chemistry as the model DWDS conditions changed from flowing water to stagnation and back to flowing water did not appear to impact the surface chemistry of the iron corrosion products and therefore Sr^{2+} adsorption to γ-FeOOH.

Strontium, based on LCF results (Table 3), was also associated with $CaCO_3$, a common accessory phase in iron corrosion products (Sontheimer *et al.* 1981; Teng *et al.* 2008; Gerke *et al.* 2012; Swietlik *et al.* 2012). Sr^{2+} substituted for Ca^{2+} in the M1 sites of $CaCO_3$ grains in PTL and RM conditions and Sr^{2+} adsorbed to the surface of $CaCO_3$ grains in PTL. Even though $CaCO_3$ was not detected by XRD analysis in any of the samples, it is commonly identified in iron corrosion products from the fully operational DWDS. The water used in this study was near or at the calcite saturation index (Table 1) so the fact that Sr^{2+} was associated with $CaCO_3$ was not surprising.

Adsorption mechanisms in chloramine-disinfected model DWDS

Strontium preferentially adsorbed to α-FeOOH in PTL and RM conditions in the chloramine-disinfected model DWDS. There was basically no difference in the percentage of Sr^{2+} adsorbed to α-FeOOH in the first two conditions, PTL and RM, of the model DWDS (~57%) (Table 3). Interestingly, LCF phase distribution suggested that Sr^{2+} desorbed primarily from α-FeOOH once flow resumed (Table 3). The distribution percentage decreased from ~57 to 16% of Sr^{2+} adsorbed to α-FeOOH and the distribution percentage increased from 34.6 to 76.8% of Sr^{2+} adsorbed to γ-FeOOH, (77%) (Table 3). Changes to water chemistry during the 1-hour stagnation and the resumption of water flow influenced the surface of the iron corrosion products such that γ-FeOOH was the preferred phase for Sr^{2+} adsorption. Strontium was also associated with $CaCO_3$ by substitution for Ca^{2+} in the M1 sites of $CaCO_3$ grains in PTL and RM conditions.

Compare/contrast adsorption of Sr^{2+} in chlorine- and chloramine-disinfected model DWDS

The Sr^{2+} concentration in the chloramine-treated PTL sample was 47 mg kg^{-1} and that in the chlorine-disinfected PTL sample was 22 mg kg^{-1} (Table 2). To assess the potential for Sr^{2+} adsorption to iron corrosion products during stagnation, ARs were injected with a 100 mg l^{-1} Sr^{2+} solution, a concentration that was over two orders of magnitude higher than the concentration in the original drinking water. The higher concentration facilitated an unambiguous interpretation of adsorption during

stagnation. After iron corrosion products were exposed to a 1-hour stagnation with the Sr^{2+}-enriched solution, the concentration of Sr^{2+} in corrosion products was similar, 215 mg kg^{-1} for the chlorine-disinfected and 217 mg kg^{-1} for the chloramine-disinfected RM samples (Table 2). Once flow was resumed to both model DWDS, the concentration of Sr^{2+} in the DS samples was 30 mg kg^{-1} for the chlorine-treated model DWDS sample and 40 mg kg^{-1} for the chloramine-treated sample (Table 2).

Differences in Sr^{2+}concentrations can be directly related to the differences in the adsorption mechanisms. Sr^{2+} preferentially adsorbed to and remained associated with γ-FeOOH in the chlorine-disinfected DWDS regardless of flow conditions, i.e., flowing or stagnant (Table 3). However, Sr^{2+} preferentially adsorbed to α-FeOOH in the PTL and RM chloramine-treated samples (Table 3). In each disinfection scenario and all water flow conditions, the presence of minimal $CaCO_3$ influenced Sr^{2+} adsorption.

The main difference in the water chemistry between the two model DWDS was the oxidation-reduction potential, which was approximately 50 mV lower in the chloramine-disinfected water (Table 1). The pH also differed by approximately 0.3 to 0.6 units lower in the chloramine-disinfected model DWDS (Table 1). Adsorption of Sr^{2+} to γ-FeOOH is predictable because the average point-of-zero charge (pzc) is approximately 6.9 (Kosmulski 2001) and the average drinking water pH above 8 (Table 1). However, the extent of Sr^{2+} adsorption to α-FeOOH in the chlorine-treated PTL, RM, and DS iron corrosion product samples was not predictable because the average pzc for synthetic α-FeOOH ranges from 7.4 to 8.2 (Appel *et al.* 2003). The overall surface charge of α-FeOOH in the drinking water should be neutral to slightly positive and it is unlikely that Sr^{2+} would sorb directly to the surface of α-FeOOH. However, in mixed mineral systems, the average pzc for each mineral can be altered through particle-particle interaction (Bell *et al.* 1973; Manning & Sabine 1997; Tombácz & Szekeres 2006). Likewise, Schwertmann & Fechter (1982) found that natural α-FeOOH can have a pzc much lower (~3) than synthetic goethites as a result of slower crystallization. Strontium was likely adsorbed to α-FeOOH and γ-FeOOH surfaces by outer-sphere surface complexation (Schwertmann & Fechter 1982; Parkman *et al.* 1998; Chen & Hayes 1999; Sahai *et al.* 2000; Chen *et al.* 2006; Carroll *et al.* 2008), which may partially explain the ease with which Sr^{2+} desorbed. Despite α-FeOOH and γ-FeOOH having similar sorption complexes and similar XANES spectra, both components were necessary to produce LCF with the lowest residual error.

In the present study, corrosion products of iron oxyhydroxides were important in the accumulation of elevated Sr^{2+} concentrations in the chlorine- and chloramine-disinfected model DWDS. Association of Sr^{2+} with $CaCO_3$ was minimal, because of the low concentrations and relatively short exposure time in the ARs. Gerke *et al.* (2013) examined iron corrosion products from an approximately 90-year-old cast iron residential main that had been exposed to the same water chemistry as the chlorine-treated model DWDS. In that study, 61 to 84% of the Sr^{2+} in surface layer iron corrosion products was associated with $CaCO_3$ and up to 39% was adsorbed to α-FeOOH. Calcite was readily identifiable in the Gerke *et al.* (2013) study for the aged cast iron residential main. The absence of γ-FeOOH in the corrosion products of Gerke *et al.* (2013) may be due to the conversion of γ-FeOOH to the more stable α-FeOOH over time (Schwertmann & Taylor 1972).

Based on the combined data sets of Gerke *et al.* (2013) and the present study, it appears that Sr^{2+} preferentially adsorbed to iron oxyhydroxides in the early stages of iron corrosion product development in both chlorine- and chloramine-disinfected DWDS. However, if $CaCO_3$ precipitates out of drinking water, Sr^{2+} can bind with and/or become incorporated into the $CaCO_3$ structure as a long-term retention mechanism; even though adsorption to iron oxyhydroxides is an essential first step in this process.

CONCLUSIONS

Strontium adsorbed to iron corrosion products in chlorine- and chloramine-disinfected model DWDS, regardless of the type of disinfection, and preferentially adsorbed to iron oxyhydroxides in the early stages of iron corrosion product development in both model DWDS. Concentrations and rates of adsorbed and desorbed Sr^{2+} differed slightly based on disinfection type. These results indicate that regardless of the type of disinfection, concentrations of Sr^{2+} could be

released from iron corrosion products in DWDS during normal operations.

ACKNOWLEDGEMENTS

MRCAT operations are supported by the Department of Energy (DOE) and the MRCAT member institutions. PNC/XSD facilities at the APS, and research at these facilities, are supported by the US DOE – Basic Energy Sciences, a Major Resources Support grant from NSERC, the University of Washington, the Canadian Light Source and the APS. Use of the APS, an Office of Science User Facility operated for the US DOE Office of Science by Argonne National Laboratory, was supported by the US DOE under Contract No. DE-AC02-06CH11357. The US Environmental Protection Agency through its Office of Research and Development funded and managed a portion of the research described here. It has been subject to Agency review but does not necessarily reflect the views of the Agency. No official endorsement should be inferred. NRL publication number JA/7303—13-1740. We thank M. K. DeSantis for photographs of the iron corrosion samples. We also thank Jason Lee for insightful comments on how to improve the manuscript.

REFERENCES

Al-Jasser, A. O. 2007 Chlorine decay in drinking-water transmission and distribution systems: pipe service age effect. *Water Res.* **41**, 387–396.

Appel, C., Ma, L. Q., Dean Rhue, R. & Kennelley, E. 2003 Point of zero charge determination in soils and minerals via traditional methods and detection of electroacoustic mobility. *Geoderma* **113**, 77–93.

Bell, L. C., Posner, A. M. & Quirk, J. P. 1973 The point of zero charge of hydroxyapatite and fluorapatite in aqueous solutions. *J. Colloid Interface Sci.* **42**, 250–261.

Boyd, G. R., Dewis, K. M., Korshin, G. V., Reiber, S. H., Schock, M. R., Sandvig, A. M. & Giani, R. 2008 Effects of changing disinfectants on lead and copper release. *J. Amer. Water Works Assoc.* **100**, 75–87.

Carroll, S. A., Roberts, S. K., Criscenti, L. J. & O'Day, P. A. 2008 Surface complexation model for strontium sorption to amorphous silica and goethite. *Geochem. Trans.* **9**, 1–26.

Chen, C. & Hayes, K. F. 1999 X-ray absorption spectroscopy investigation of aqueous Co(II) and Sr(II) sorption at clay-water interfaces. *Geochim. Cosmochim. Acta* **63**, 3205–3215.

Chen, C., Coleman, M. L. & Katz, L. E. 2006 Bridging the gap between macroscopic and spectroscopic studies of metal ion sorption at the oxide/water interface: Sr(II), Co(II), and Pb(II) sorption to quartz. *Environ. Sci. Technol.* **40**, 142–148.

Cornell, R. M. & Schwertmann, U. 2003 *The Iron Oxides; Structure, Properties, Reactions, Occurrences and Uses*. Wiley-VCH Verlag GmbH & Co. KGaA, Weinheim.

Eikenberga, J., Triccab, A., Vezzua, G., Stilleb, P., Bajoa, S. & Ruethi, M. 2001 $^{228}Ra/^{226}Ra/^{224}Ra$ and $^{87}Sr/^{86}Sr$ isotope relationships for determining interactions between ground and river water in the upper Rhine valley. *J. Environ. Radioact.* **54**, 133–162.

Friedman, M. J., Hill, A. S., Reiber, S. H., Valentine, R. L., Larsen, G., Young, A., Korshin, G. V. & Peng, C. Y. 2010 *Assessement of Inorganics Accumulation in Drinking Water System Scales and Sediments*. Water Research Foundation, Denver, CO.

Gerke, T. L., Maynard, J. B., Schock, M. R. & Lytle, D. A. 2008 Physio-chemical characterization of five iron tubercles from a single drinking water distribution system: possible new insights on their formation and growth. *Corros. Sci.* **50**, 2030–2039.

Gerke, T. L., Scheckel, K. G. & Maynard, J. B. 2010 Speciation and distribution of vanadium in drinking water iron pipe corrosion by-products. *Sci. Total Environ.* **408**, 5845–5853.

Gerke, T. L., Scheckel, K. G., Ray, R. I. & Little, B. J. 2012 Can dynamic bubble templating play a role in corrosion product morphology? *Corrosion: J. Sci. Engin.* **68**, 02004-02001–025004-025007.

Gerke, T. L., Little, B. J., Luxton, T. P., Scheckel, K. G. & Maynard, J. B. 2013 Strontium concentrations in corrosion products from residential drinking water distribution systems. *Environ. Sci. Technol.* **47** (10), 5171–5177.

Heald, S. M., Brewe, D. L., Stern, E. A., Kim, K. H., Brown, F. C., Jiang, D. T., Crozier, E. D. & Gordon, R. A. 1999 XAFS and micro-XAFS at the PNC-CAT beamlines. *J. Synch. Rad.* **6**, 347–349.

Kosmulski, M. 2001 *Chemical Properties of Material Surface*. Vol. 102. Marcel Dekker, Inc., New York.

Kropf, A., Katsoudas, J., Chattopadhyay, S., Shibata, T., Lang, E., Zyryanov, V., Ravel, B., McIvor, K., Kemner, K., Scheckel, K., Bare, S., Terry, J., Kelly, S., Bunker, B. & Segre, C. 2009 The New MRCAT (Sector 10) Bending Magnet Beamline at the Advanced Photon Source (R. Garrett, I. Gentle, K. Nugent & S. Wilkins, eds). 10th International Conference on Synchrotron Radiation Instrumentation, Melbourne, Australia, pp. 299–302.

Lin, Y. P. & Valentine, R. L. 2009 Reduction of lead oxide (PbO_2) and release of Pb(II) in mixtures of natural organic matter, free chlorine and monochloramine. *Environ. Sci. Technol.* **43**, 3872–3877.

Lin, J., Ellaway, M. & Adrien, R. 2001 Study of corrosion material accumulated on the inner wall of steel water pipe. *Corros. Sci.* **43**, 2065–2081.

Manning, B. A. & Sabine, G. 1997 Adsorption and stability of arsenic (III) at the clay mineral-water interface. *Environ. Sci. Technol.* **31**, 2005–2011.

O'Day, P., Newville, M., Neuhoff, P., Sahai, N. & Carrol, S. 2000 X-ray absorption spectroscopy of strontium(II) coordination I. Static and thermal disorder in crystalline, hydrated, and precipitated solids and in aqueous solution. *J. Colloid Interface Sci.* **222**, 184–197.

Parkman, R. H., Charnock, J. M., Livens, F. R. & Vaughan, D. J. 1998 A study of the interaction of strontium ions in aqueous solution with the surfaces of calcite and kaolinite. *Geochim. Cosmochim. Acta* **62**, 1481–1492.

Peng, C. Y. & Korshin, G. V. 2011 Speciation of trace inorganic contaminants in corrosion scales and deposits formed in drinking water distribution systems. *Water Res.* **45**, 5553–5563.

Peng, C. Y., Ferguson, J. F. & Korshin, G. V. 2013 Effects of chloride, sulfate and natural organic matter (NOM) on the accumulation and release of trace-level inorganic contaminants from corroding iron. *Water Res.* **47**, 5257–5269.

Ravel, B. & Newville, M. 2005 ATHENA, ARTEMIS, HEPHAESTUS: data analysis for X-ray absorption spectroscopy using IFEFFIT. *J. Synch. Rad.* **12**, 537–541.

Sahai, N., Carroll, S. A., Roberts, S. & O'Day, P. A. 2000 X-ray absorption spectroscopy of strontium(II) coordination. II. Sorption and precipitation at kaolinite, amorphous silica, and goethite surfaces. *J. Colloid Interface Sci.* **222**, 198–212.

Sarin, P., Snoeyink, V. L., Lytle, D. A. & Kriven, W. M. 2004 Iron corrosion scales: model for scale growth, iron release and colored water formation. *J. Environ. Eng.* **130**, 364–373.

Schock, M. R. & Lemieux, F. G. 2010 Challenges in addressing variability of lead in domestic plumbing. *Water Sci. Technol.: Water Supply* **10** (5), 793–799.

Schwertmann, U. & Fechter, H. 1982 The point of zero charge of natural and synthetic ferrihydrites and its relation to adsored silicate. *Clay Miner.* **17**, 471–476.

Schwertmann, N. U. & Taylor, R. M. 1972 The transformation of lepidocrocite to goethite. *Clays Clay Miner.* **20**, 151–158.

Sedlak, D. L. & von Gunten, U. 2011 The chlorine dilemma. *Science* **331** (6013), 42–43.

Segre, C., Leyarovska, N., Chapman, L., Lavender, W., Plag, P., King, A., Kropf, A., Bunker, B., Kemner, K., Dutta, P., Duran, R. & Kaduk, J. 1999 The MRCAT insertion device beamline at the Advanced Photon Source. In *Synchrotron Radiation Instrumentation* (P. Pianetta, J. Arthur & S. Brennan, eds). Stanford, CA, pp. 419–422.

Shaw, B. W., Rubinstein, C. & Baker, T. 2012 Rules and regulations for public water systems. In *Division* (B. W. Shaw, ed.). Texas Commission on Environmental Quality, Austin, TX, 2012, p. 114.

Sontheimer, H., Kolle, W. & Snoeyink, V. L. 1981 The siderite model of the formation of corrosion-resistant scales. *J. Amer. Water Works Assoc.* **73**, 572–579.

Swietlik, J., Raczyk-Stanislawiak, U., Piszora, P. & Nawrocki, J. 2012 Corrosion in drinking water pipes: the importance of green rusts. *Water Res.* **46**, 1–10.

Szabo, J. G., Impellitteri, C. A., Govindaswamy, S. & Hall, J. S. 2009 Persistence and decontamination of surrogate radioisotopes in a model drinking water distribution system. *Water Res.* **43**, 5005–5014.

Tamura, H. 2008 The role of rusts in corrosion and corrosion protection of iron and steel. *Corros. Sci.* **50**, 1872–1883.

Tang, Z., Hong, S., Xiao, W. & Taylor, J. 2006 Characteristics of iron corrosion scales established under blending of ground, surface, and saline waters and their impacts on iron release in the pipe distribution system. *Corros. Sci.* **48**, 322–342.

Teng, F., Guan, Y. T. & Zhu, W. P. 2008 Effect of biofilm on cast iron pipe corrosion in drinking water distribution system: Corrosion scales characterization and microbial community structure investigation. *Corros. Sci.* **50**, 2816–2823.

Tombácz, E. & Szekeres, M. 2006 Surface charge heterogeneity of kaolinite in aqueous suspension in comparison with montmorillonite. *Appl. Clay Sci.* **34**, 105–124.

USEPA 2009 *Contaminant Information Sheets for the Final CCL 3 Chemicals*. Vol. EPA 815-R-09-012. USEPA, Washington, DC, 214.

USEPA 2012 *Unregulated Contaminant Monitoring Rule 3 (UCMR 3)*. Vol. 77FR26071. USEPA, Washington, DC, pp. 26071–26101.

Vikesland, P. J. & Valentine, R. L. 2002 Iron oxide surface-catalyzed oxidation of ferrous iron by monochloramine: Implications of oxide type and carbonate on reactivity. *Environ. Sci. Technol.* **36**, 512–519.

Watts, P. & Howe, P. 2010 Strontium and strontium compounds. *Concise International Chemical Assessment, Document* **77**, 63.

Zhang, Y. & Edwards, M. 2007 Anticipating effects of water quality changes on iron corrosion and red water. *J. Water Supp.: Res. Tech. – AQUA* **5**, 55.

First received 12 April 2013; accepted in revised form 19 December 2013. Available online 4 February 2014